The anodic dissolution of copper alloys: Pure copper in synthetic tap water

P. Zhou[a], M.J. Hutchison[b], J.R. Scully[b], K. Ogle[a],*

[a] Ecole Nationale Supérieure de Chimie de Paris, IRCP, CNRS, 11 Rue Pierre et Marie Curie, Paris 75005, France
[b] Department of Materials Science and Engineering, University of Virginia, 395 McCormick Road, Charlottesville, VA 22904, USA

A B S T R A C T

The anodic dissolution of pure copper was investigated in naturally aerated synthetic tap water (STW) by in situ atomic emission spectroelectrochemistry (AESEC). This technique measures the Cu dissolution rate directly and the formation of Cu scale indirectly by mass balance between the anodic current and the dissolution rate. The conditions investigated include the effect of applied current (0–80 μA) and time duration at 40 μA (0–20 min). Oxide scale formed during exposure to STW was dissolved in a deaerated citrate buffer solution (CBS) and followed by in situ AESEC as well. A mass/charge balance confirmed the predication that most Cu(II) species are soluble and are released into STW, leaving behind a Cu_2O film as an insoluble product on the surface. Ex situ Raman spectroscopy and grazing incidence X-ray diffraction analysis (GIXRD) also corroborate this conclusion. A quantitative analysis of Cu(I) and Cu(II) species vs. applied current and vs. time during a galvanostatic pulse are presented. At open circuit the oxidation product is essentially Cu_2O; soluble Cu(II) is favored as anodic polarization is increased. A kinetic analysis suggests that the dissolution mechanism involves simultaneous Cu dissolution and film formation rather than a sequential mechanism.

© 2016 Elsevier Ltd. All rights reserved.

1. Introduction

The corrosion of copper (Cu) and its alloys is a troublesome problem due to their large-scale use in potable water plumbing systems[1–14] resulting in the premature failure of tubes and fittings, toxicity due to Cu release, and costly expenses involved in waste water disposal. Besides the sporadic tubercle blockages due to the deposition of scales, superfluous soluble Cu release into water not only causes serious health problems [1], but induces accelerated corrosion elsewhere in iron pipelines [13], which are also largely utilized in water distribution system. To date, much work has been conducted to investigate factors that affect corrosion of copper and its alloys. Water chemistry [3,12,13], surface states of sample [2], temperature [6,15] and pretreatment [16], all affect the corrosion of Cu and its alloys in a complicated way, to the extent that data from field work often contradicts results from laboratory work. In order to unravel the source of these controversies, a clear mechanistic explanation of the corrosion process is indispensable.

There are many mechanistic explanations of copper corrosion in the literature including the one-electron and the two-electron reaction mechanisms [8,17,18,36]. The one-electron reaction mechanism describes the corrosion behavior of Cu such that cuprite is the direct reaction product deposited on copper, and soluble species are released by further reaction of cuprite into Cu (II) species [19,20]. However, other workers have inferred that copper was oxidized into Cu(II) species directly [6], resulting in an equilibrium state between the Cu(II) species and Cu(I) species by disproportionation of Cu(I) or synproportionation between Cu(0) and Cu(II) [2,4,8] [21–23]. It is commonly accepted that cuprite (Cu_2O) forms on the surface and constitutes a non-protective scale during the corrosion of copper in tap water [11,24]. Some researchers found trace amounts of precipitated Cu(II) species such as $Cu(OH)_2$ and malachite ($Cu_2CO_3(OH)_2$) [8,25], however these species were mostly produced in high alkalinity water or after a long period of immersion. The theory that cuprite is the predominant insoluble corrosion product has been popularly proposed [36,39]. But the origin of Cu_2O and its interrelationship to the soluble species is still unclear.

The addition of saline constituents into water, together with dissolved oxygen and organic matter, exacerbate the corrosivity of typical tap water [26–30]. Cations such as K^+, Na^+ and Ca^{2+} exhibit a minor effect on water corrosivity [31], though Ca^{2+} is believed to

* Corresponding author.
E-mail address: kevin.ogle@chimie-paristech.fr (K. Ogle).

Nomenclature

C_{Cu}	Cu concentration as measured by ICP-OES (various units)
i_{ap}	Applied current during galvanostatic experiment (nA)
E	Potential (V vs. SCE)
f	Flow rate of electrolyte through electrochemical cell ($cm^3 s^{-1}$)
$h(t)$	Residence time distribution for the electrochemical flow cell (unitless)
τ	Empirical parameter for log-normal fit (s)
β	Empirical parameter for log-normal fit (unitless)
n_{aq}	Number of electrons transferred to form aqueous Cu species (no unit)
n_s	Number of electrons transferred to form solid Cu species (no unit)
t	Time (s)
F	Faraday constant (=96500C mol^{-1})
ν	Instantaneous rate of a reaction (nmol s^{-1})
$\nu_{Cu(aq)}$	Dissolution rate of Cu into aqueous species (nmol s^{-1})
$\nu_{corr(aq)}$	Spontaneous dissolution rate at open circuit (nmol s^{-1})
ν_{Cu2O}	Growth rate of residual oxide film on Cu surface (nmol s^{-1})
ν_e	Applied current expressed as transfer rate of electrons (nmol s^{-1})
$\nu_e{}^*$	ν_e after convolution with h(t) (nmol s^{-1})
Q	Quantity of substance (nmol)
$Q_{Cu(aq)}$ (el)	Quantitiy of Cu released during an experiment in a specific electrolyte (el)
$Q_{an(aq)}$	Quantity of dissolved Cu attributed to the galvanostatic current (nmol)
$Q_{corr(aq)}$	Quantity of dissolved Cu attributed to spontaneous dissolution (nmol)
$Q_{an(s)}$	Quantity of Cu formed as an oxide film due to galvanostatic current (nmol)
$Q_{corr(s)}$	Quantity of Cu formed as an oxide film due to corrosion (nmol)
Q_e (pstat)	Quantity of electricity obtained by integrating the current transient (nmol)
Q_e (ICP)	Quantity of equivalent electricity from ICP-OES data assuming a specific stoichiometry

form calcium carbonate that can mitigate corrosion [32,33]. Anions such as Cl^- and $SO_4{}^{2-}$ are oxidants that copper corrosion [12,34]. However, the synergistic effect among these anions is complex [11,12,27], and these mechanistic speculations are less reliable in predicting Cu corrosion. Some researchers have tried to quantitatively explore the relationship of insoluble and soluble species [35]: Xiao et al [8]. tried to explain copper corrosion by differentiating peaks among the X-ray photoelectron spectra (XPS); Feng [36], M. Drogowska [37], Nakayama [38] used a small cathodic current to the solid corrosion products and to identify the corrosion products based on the potential features of the potential vs. time curve, and determine their relative proportions through charge conservation. However, XPS analysis is only a semi-quantitative method and galvanostatic cathodic reduction has poor time resolution [38]. In addition, the nature of the residual oxide film may play an important role in the dissolution mechanism, especially for a porous or defect-rich structure [24]. Hultquist and Szakalos proposed the existence of hydrogen

evolution via water reduction during Cu corrosion in anoxic pure water [15,39–42], which was considered to be thermodynamically unlikely and thereby disputed [43–45]. In principle, this phenomenon could be explained by the catalytic property of the corrosion product produced through the one-electron mechanism [44]. A similar idea was proposed by Jacobs and Edwards [46], who evoked the catalyzing nature of sulfide in Cu corrosion.

In this paper, the anodic dissolution of Cu in synthetic tap water (STW) (pH = 7.5 ± 0.1) was investigated using *in situ* atomic emission spectroelectrochemistry (AESEC) to monitor Cu dissolution directly and scale formation by mass balance. In this way it is possible to access the question of Cu dissolution stoichiometry directly. In future work, the approach described here will be extended to investigate the dezincification of Cu-Zn alloys.

2. Experimental

2.1. Materials

Oxygen-free, high thermal conductivity Cu (Goodfellow, purity: 99.95+ %;) was used in this work. The material was cut into 25 mm × 25 mm × 3 mm specimens and ground with 400 and 600 grit SiC paper, rinsed with deionized water, degreased with acetone, ethanol, and then dried under flowing nitrogen.

Synthetic tap water (STW) [47] containing 200 mg L^{-1} $SO_4{}^{2-}$, 50 mg L^{-1} Cl^-, 30.5 mg L^{-1} $HCO_3{}^-$, 27.9 mg L^{-1} Ca^{2+}, 3.4 mg L^{-1} Mg^{2+}, and 101.2 mg L^{-1} Na^+ was prepared using reagent grade chemicals and deionized water (Millipore™ system, 18.2 Ω cm at 25 °C). The anion composition in this STW was taken from [47], however, cations like Ca^{2+} and Mg^{2+} were partially replaced by Na^+ so as to simulate a soft tap water after being ion exchanged from a hard tap water. The STW has an alkalinity of 84 mg L^{-1} as $CaCO_3$ and its pH and conductivity were 7.5 ± 0.1 and 479 μS cm^{-1}, respectively.

A citrate buffer solution (CBS) with pH = 5.0 ± 0.1 was used to dissolve corrosion products formed on the surface after exposure to STW. It was prepared with 0.1 M citric acid solution (AppliChem) and 0.1 M sodium citrate solution (Amresco), and then mixed to achieve the target pH value. Unless otherwise noted, all the citrate buffer solutions were de-aerated for at least 30 min by Ar bubbling and were used under flowing Ar.

2.2. Instrumentation

A custom designed flow cell, described in detail elsewhere [48–50], was used for these experiments. A platinum plate with a geometry area of 5 cm^2 and a saturated calomel electrode (SCE) were used as the counter and reference electrode, respectively. The Cu specimens were used as the working electrode with a surface area of 1 cm^2 defined by the geometry of the o-ring. A flow rate $f = 3$ $cm^3 min^{-1}$ was used. All experiments were conducted at ambient temperature of approximately 25 °C. A potentiostat (Gamry Reference 600™) was used to control current or potential and monitor the open circuit potential.

AESEC was used to monitor the instantaneous concentrations of Cu and other ions downstream from the flow cell using an inductively coupled plasma atomic emission spectrometer (ICP-AES, Horiba Jobin Yvon, Ultima 2™). Details of this system may be found in previous work [48]. The copper dissolution was followed using a monochromator to detect the emission intensity of the 324.75 nm line of atomic Cu with a typical detection limit of less than 1 ppb under the conditions of our experiment. The detection limit was here defined as three times the standard deviation of the blank measured over 100 s, with a 1 s integration time per point. All the AESEC experiments were calibrated using three standards

(10 ppb, 20 ppb, 30 ppb of Cu in STW and 20 ppb, 50 ppb, 80 ppb of Cu in CBS) with a correlation coefficient $R^2 \geq 0.99$.

Bulk sample X-ray diffraction (XRD), grazing incidence X-ray diffraction (GIXRD) and Raman spectroscopy were used to analyze the residual Cu oxide film following exposure of Cu to STW with a galvanostatic current of 80 μA for 1200 s. Diffraction experiments were performed on a PANalytical X'Pert Diffractometer with a Cu target (Kα = 1.54 Å). A fixed incident angle of 0.5° (ω = 0.5°) was used to limit the excitation depth into the sample. Crystalline surface oxides were analyzed using GIXRD. Bulk XRD of samples was performed using a spinning sample stage. The same sample was also used to obtain Raman spectra with a Renishaw InVia Raman microscope consisting of a 514 nm Ar ion Laser in 180° backscattering geometry, and a 3000 g/mm grating. The laser illuminated spot diameter was approximately 1 μm focused through a 50 × 0.75 NA objective. Pressed Cu_2O powder reference was prepared and investigated with a 488 nm laser.

2.3. Data Analysis

We may assume that Cu oxidation leads to the formation of both soluble and insoluble corrosion products. The formation of soluble corrosion products is monitored as the Cu dissolution rate, $v_{Cu(aq)}$ (nmol s^{-1}). This value is determined directly from the downstream Cu concentration by Eq. (1):

$$v_{Cu(aq)} = f C_{Cu} \tag{1}$$

where f is the flow rate of the electrolyte (cm^3 s^{-1}) and C_{Cu} is the downstream concentration of Cu determined from the spectral emission, and the abbreviation aq specifies the aqueous (dissolved) species. The electrical current was measured simultaneously. In order to compare the two values on a quantitative scale, it is useful to convert the current to an electron transfer rate (nmol e$^-$ s^{-1}):

$$v_e = i_{ap}/F \tag{2}$$

where i_{ap} is the applied electrical current (nA) and F is the Faraday constant. This conversion is used for stoichiometric analysis since converting the dissolution rates into equivalent currents requires an assumption of the oxidation state of the dissolved Cu.

For a mass balance it is often of interest to use an integrated form of Eqs. (1) and (2) which yields the quantity (nmol), Q, of either copper or electrons. For example, the total quantity of Cu dissolved in STW will be referred to as $Q_{Cu(aq)}$ *(STW)* while the total quantity of electrons passing through the potentiostat will be referred to as Q_e *(pstat)*. Other terms useful for mass/charge balance will be defined as needed.

For kinetic measurements, it is important to consider the time resolution of the experiment. Eqs. (1)–(2) are written in terms of instantaneous variables. Indeed, the electrical current may be considered to be an instantaneous measurement on the time scale of these experiments, however the Cu dissolution transients will be broadened by the residence time distribution, $h(t)$, in the electrochemical flow cell [50]. The extensive diffusion layer and low convection rate result in a significant broadening of the concentration transient with respect to v_e, leading to a convolution integral relationship between v_e and v_e^*:

$$v_e{}^*(t) = \int_0^t v_e(x)\, h(t-x)\, dx \tag{3}$$

Experimental measurement of the $h(t)$ from pulse dissolution experiments has shown that it closely follows a log normal distribution:

$$h(t) = \sqrt{\frac{\beta}{\pi \tau^2}} e^{-\frac{1}{4\beta}} e^{-\beta \ln^2 (t/\tau)} \tag{4}$$

where τ and β are empirically determined parameters. In this work, $\tau = 10.2$ s and $\beta = 0.99$ were used as determined from a previously published variation of h(t) with flow rate [50].

3. Results

3.1. Mass and Charge Balance in Acid Electrolytes

It was of interest to validate Eqs. (1) and (2) under conditions in which the oxidation states of dissolved Cu are well known. This was achieved by performing galvanostatic dissolution experiments in deaerated 0.6 M HCl and 1.5 M H_2SO_4, for which an $n = 1$ and an $n = 2$ dissolution mechanism have been observed [49], respectively. Typical dissolution profiles are given in Fig. 1. These profiles are divided into three periods: For $t < 0$ and for $t > 300$ s, the Cu specimen reacted with the electrolyte at open circuit and the
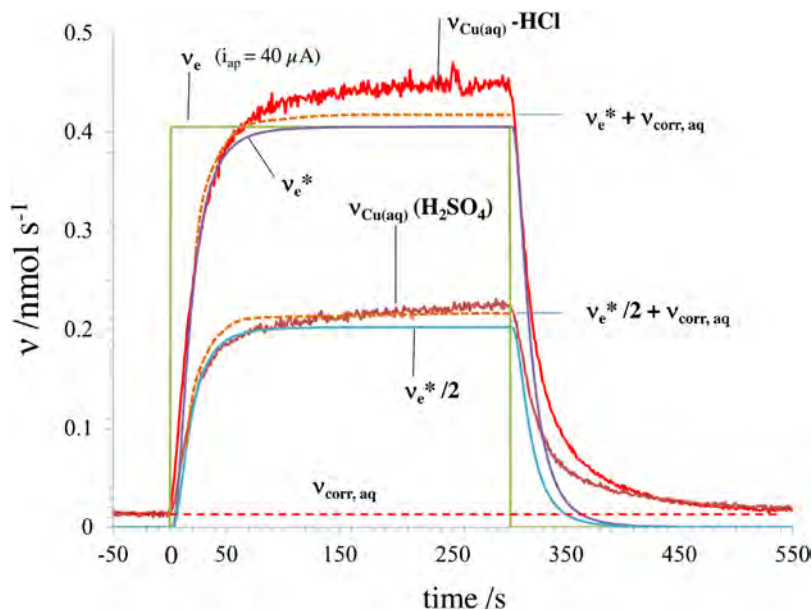

Fig. 1. Typical Cu dissolution transients at open circuit and during a 40 μA galvanostatic pulse for a 300 s in deaerated 1.5 M HCl and 0.6 M H_2SO_4.

corrosion rate, $v_{corr(aq)}$, was estimated from the steady state Cu concentration by Eq. (1) during the open circuit periods, assuming only soluble Cu corrosion products. The open circuit dissolution rate was measured for 20 minutes prior to $t = 0$, although Fig. 1 shows only the final 50 s of this exposure.

At $t = 0$, a galvanostatic pulse of 40 μA was applied for a duration of 300 s, followed by a return to the open circuit potential for 300 s. The spontaneous soluble corrosion rate, $v_{corr(aq)}$, was determined to be approximately 0.015 nmol s^{-1} for 0.6 M HCl and 0.014 nmol s^{-1} in H$_2$SO$_4$ prior to the anodic pulse. Following the pulse, the Cu signal returned after about 200 s to a value that was nearly identical within experimental error.

The original current, v_e, and the convoluted current, v_e^* are both given in Fig. 1. The dashed curve shows $v_e^* + v_{corr(aq)}$, which allows a comparison between the dissolution rate and the current corrected for the background corrosion rate. For 0.6 M HCl electrolyte, it is observed that $v_{Cu(aq)}$ and $v_e^* + v_{corr(aq)}$ follow each other closely indicative of an $n = 1$ mechanism. For 1.5 M H$_2$SO$_4$ the AESEC results are compared with $v_e^*/2$ in anticipation of an $n = 2$ mechanism and again the good correlation between $v_{Cu(aq)}$ and $v_e^*/2 + v_{corr(aq)}$ confirms this hypothesis.

The ability of the AESEC technique to quantitatively estimate the n value for anodic dissolution is demonstrated by the mass balance in Fig. 2. To produce this analysis, a series of anodic galvanostatic pulses were applied to the sample ranging from $i_{ap} = 5$ μA to 100 μA of $\Delta t = 300$ s, with a 300 s open circuit delay between each pulse. The quantity of electricity, Q_e (pstat), was obtained by integrating the current transient, which under galvanostatic conditions is simply:

$$Q_e \text{ (pstat)} = i_{ap} \, \Delta t / F \quad (5)$$

To determine the n value, it is necessary to compare Q_e(pstat) with the quantity of Cu released by the anodic current, $Q_{an(aq)}$. The latter was determined from the total amount of Cu dissolved during the anodic pulse, $Q_{Cu(aq)}$, by subtracting the integral of the estimated spontaneous corrosion rate $Q_{corr(aq)}$:

$$Q_{an(aq)} = Q_{Cu(aq)} - Q_{corr(aq)} \quad (6)$$

Q_{corr} was estimated by assuming that the spontaneous dissolution rate is identical during the anodic pulse as that measured prior to the anodic pulse:

$$Q_{corr(aq)} = v_{corr(aq)} \, \Delta t \quad (7)$$

From a mass/charge balance:

$$Q_e \text{ (pstat)} = n \, Q_{an(aq)} = Q_e \text{ (ICP)} \quad (8)$$

The experimental data are shown as discrete data points. The hypothetical lines predicted for an $n = 1$ and $n = 2$ mechanism are shown as solid lines. The average experimental stoichiometry factor in this current range was 1.81 for copper dissolution in H$_2$SO$_4$, while $n = 1.06$ was measured in 1.5 M HCl.

3.2. The STW–CBS Dissolution Experiment

The experimental protocol for Cu in STW was identical to that previously presented for Cu dissolution in acid solutions however a direct mass balance may not be performed because a significant quantity of insoluble Cu corrosion products are formed. Therefore, following the STW experiment, the STW electrolyte was exchanged for the CBS electrolyte with the idea of dissolving any residual oxide films that may have formed on the surface during the STW experiment.

A typical dissolution profile for a STW–CBS experiment is shown in Fig. 3. Again, v_e, v_e^*, and $v_{Cu(aq)}$ are given as a function of time along with the potential, E (vs. SCE). The experiment is divided into four periods. (a) Firstly, the Cu specimen was allowed to react with STW for 300 s at open circuit during which period the spontaneous rate of Cu dissolution, $v_{corr(aq)}$, was measured. (b)
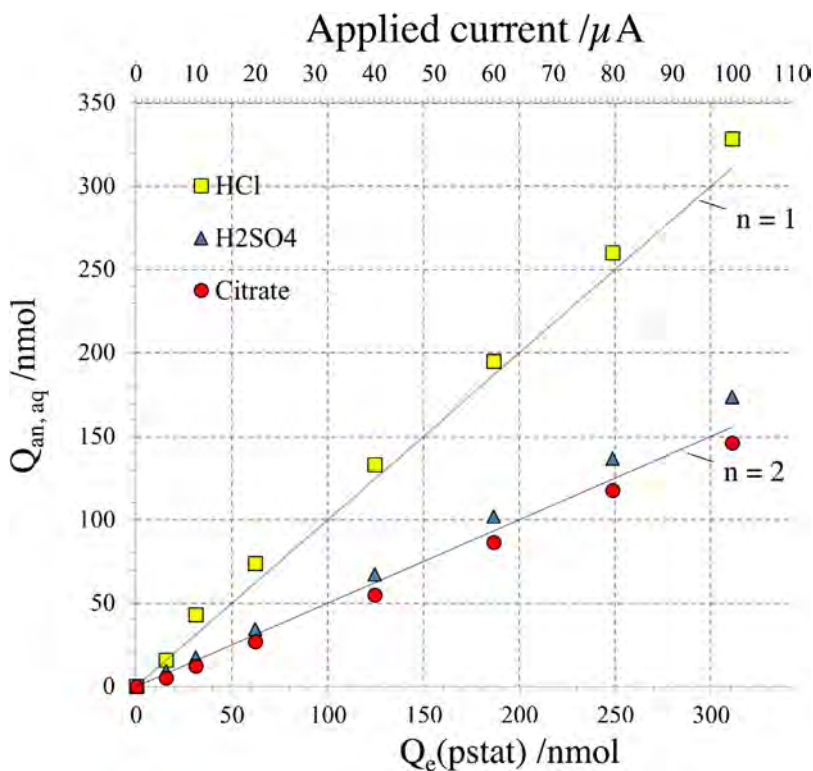

Fig. 2. $Q_{an(aq)}$ vs. Q_e(pstat) as measured from a stepwise galvanostatic dissolution experiments in the range of applied current from 0 to 100 μA in HCl (□), H$_2$SO$_4$ (△), and citrate buffer solution (○).
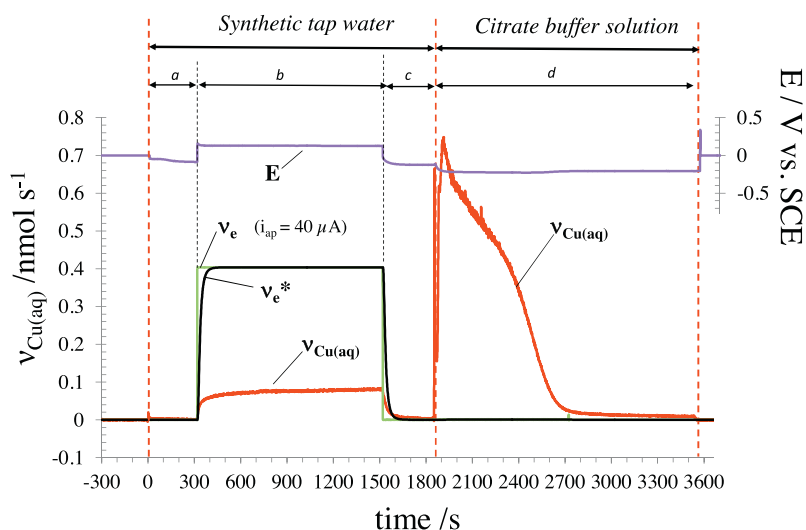
Fig. 3. Typical anodic dissolution of copper in STW, followed by open circuit dissolution of residual oxide film in citrate buffer solution (STW-CBS experiment). Four time periods are shown: (a) initial open circuit for 300 s in STW; (b) Anodic polarization of copper in STW, i_{ap} = 40 μA, Δt = 1200 s; (c) return to open circuit dissolution for 300 s in STW; (d) CBS was introduced to naturally dissolve the residual scale on surface.

Next, a galvanostatic pulse of i_{ap} = 40 μA was applied for Δt = 1200 s. This period was associated with a large positive shift in E due to the high resistivity of the STW electrolyte. Note that throughout this period, $v_{Cu(aq)} << v_e^*$, which implies that an insoluble film was formed during the STW exposure. (c) Next, the sample was returned to the open circuit potential again for 300 s. (d) Finally the dissolution of the solid film was performed at open circuit in the CBS electrolyte.

The initial open circuit dissolution of copper in STW (see the expanded scale version in Fig. 4) was very slow with an average value of $v_{Cu(aq)}$ of approximately $2 \pm 1 \times 10^{-2}$ nmol s^{-1} during this period, corresponding to an average steady state concentration of about 2.6 ppb Cu. This is very close to the detection limit of approximately 1 ppb, although clearly detectable as seen in Fig. 4.

During the galvanostatic pulse (stage b), $v_{Cu(aq)}$, increased rapidly during the first 100 s and then rose very slowly to obtain 0.080 ± 0.004 nmol s^{-1} by the end of the experiment. $v_{Cu(aq)}$ is

however much less than v_e^* throughout the anodic pulse indicative of the formation of insoluble Cu oxidation products. The second open circuit delay in STW (stage c) showed a rapid decrease of Cu to a value that is comparable to the initial open circuit dissolution rate. The result suggests that the scale formed during anodic polarization does not significantly alter the spontaneous corrosion rate of Cu.

In order to estimate the quantity of scale formed during the polarization, the sample was then exposed to deaerated citrate buffer solution (CBS) (stage d). This electrolyte was chosen because citrate is a common reagent used in Cu and brass descaling formulations [51]. Cu dissolution reached a maximum within 50 s, followed by a sharp decrease for 900 s. A subsequent steady state dissolution of Cu was observed afterwards. The onset of scale dissolution coincided with a sharp drop of E to about −0.22 V vs. SCE, followed by a slight rise to −0.20 V vs. SCE. By the end of the experiment, the average $v_{Cu(aq)}$ was approximately 0.01 nmol s^{-1}.
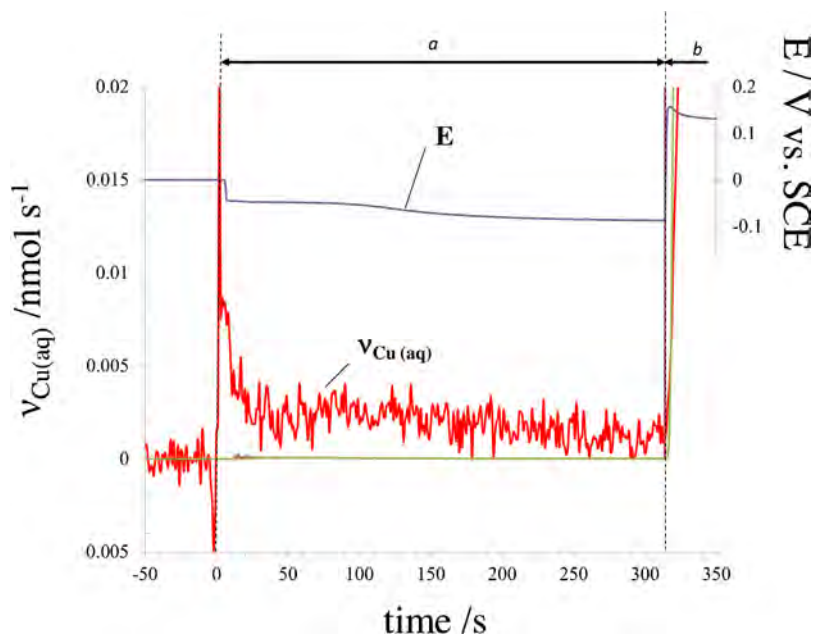

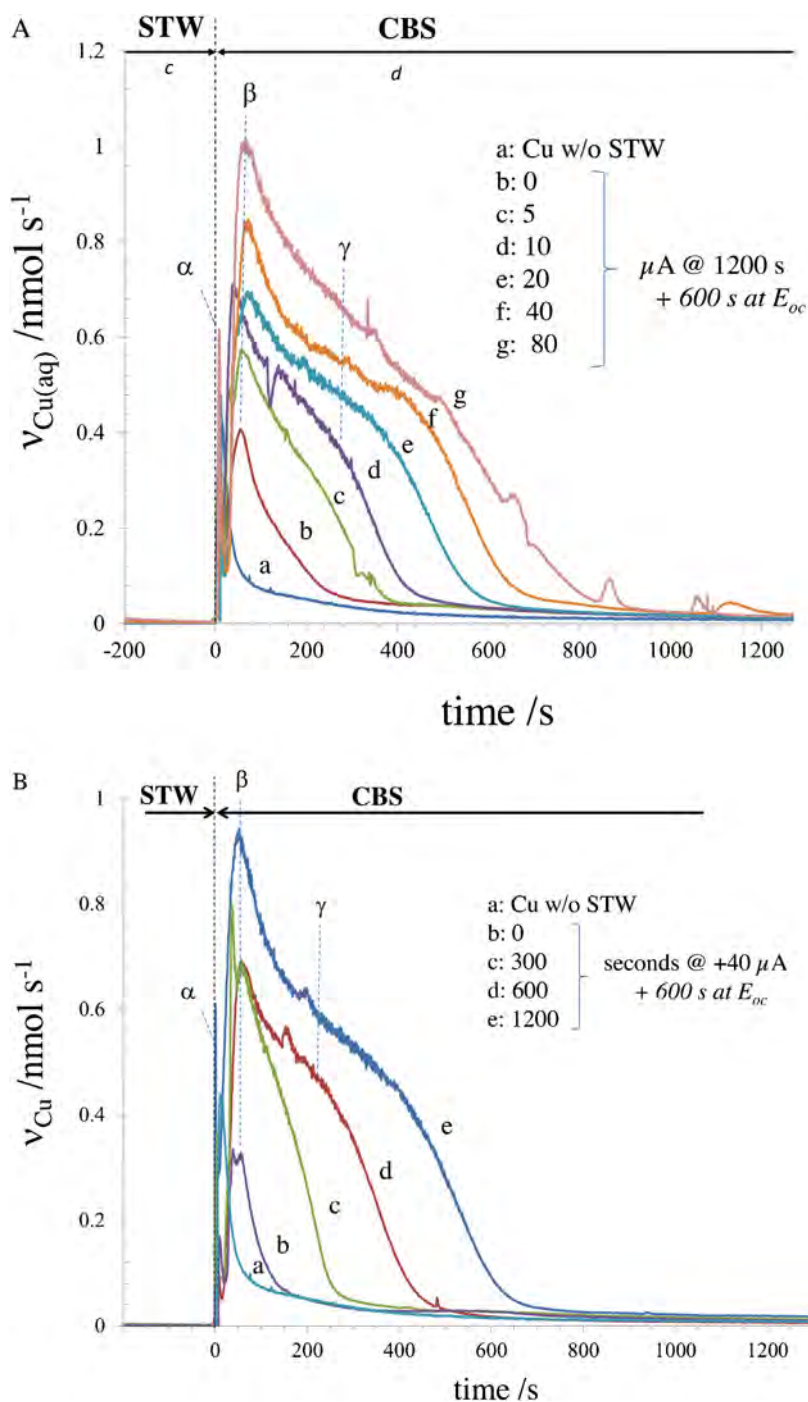**Fig. 4.** Enlarged view of the open circuit dissolution period (stage (a) in Fig. 3).

Fig. 5. Growth of the Cu dissolution transient in CBS with increasing anodic polarization in STW showing three transient features labeled α, β, and γ. All STW experiments included 600 s of open circuit exposure in addition to the galvanostatic pulse.
(A) Variable i_{ap} with $\Delta t = 1200$ s: a- fresh copper with no STW exposure; b- 0 μA; c- 5 μA; d- 10 μA; e- 20 μA; f- 40 μA; g- 80 μA.
(B) Variable Δt with $i_{ap} = 40$ μA. a: fresh copper with no STW exposure; b: $\Delta t = 0$ min; c: 5 min; d: 10 min; e: 20 min.

The experiment of Fig. 3 was conducted for variable applied current, i_{ap}, for an anodic polarization time of $\Delta t = 1200$ s (Fig. 5A); and a variable Δt at $i_{ap} = 40$ μA cm^{-2} (Fig. 5B). For clarity, only the CBS dissolution step is shown in Fig. 5. The dissolution profile of pure Cu exposed to CBS electrolyte without any exposure to STW (curve a in Fig. 5A/B) is also shown as a reference. For all experiments involving STW exposure, the total duration of the open circuit period (a + c) was maintained constant at 600 s as in Fig. 3.

At least three distinct features are observed in the dissolution profiles of Fig. 5 which for convenience we have labeled α, β and γ. A sharp peak (α) occurs immediately when the CBS electrolyte contacts the Cu surface. This is particularly noticeable, and is in fact the only peak observed, for the uncorroded Cu specimen. This is followed by a slow and broad dissolution that is itself divided into two features: a rather rapid maximum (β) and a very broad shoulder (γ). Following this, ultimately $\nu_{Cu(aq)}$ returns to a steady state value of 0.014 ± 0.003 nmol s^{-1} where the error represents the standard deviation of all the experiments of Fig. 5. Note that

this value is comparable to open circuit dissolution rates observed in deaerated 0.6 M H_2SO_4 and 1.5 M HCl. The unexposed Cu surface shows only a sharp peak at the origin and falls off slowly to obtain $v_{Cu(aq)} = 0.010 \pm 0.002$ nmol s^{-1}, somewhat lower but comparable to that of the other surfaces.

The second, broad peak undergoes a systematic growth with either increasing applied current or increasing time and is absent for the surface without exposure to STW. This clearly demonstrates that Cu dissolution in the second peak in the CBS electrolyte may be attributed to the formation of a residual film during open circuit or galvanostatic exposure to STW electrolyte.

3.3. Mass and Charge Balance for Anodic Dissolution of Cu in STW

The oxidation of Cu in the STW solution may occur via either spontaneous corrosion or by the applied anodic current and in both cases may lead to a soluble (aqueous, aq) and an insoluble (solid, s) component:

$$Total\ Cu\ oxidized\ in\ STW = Q_{corr(aq)} + Q_{corr(s)} + Q_{an(aq)} + Q_{an(s)} \quad (9)$$

As in the previous section, it is possible to investigate the stoichiometry of dissolution by a mass/charge balance. However the situation is more complex, as the solid and aqueous forms of Cu may have different oxidation states. The quantity of soluble Cu released by the anodic reaction, $Q_{an(aq)}$, may be estimated by analogy to Eq. (6). For this case however, the spontaneous corrosion is negligible. Likewise, the solid component of the anodic reaction, $Q_{an(s)}$ may be determined from:

$$Q_{an(s)} = Q_{Cu(aq)}(CBS) - Q_{Cu(aq)}(CBS)(i_{ap} = 0) \quad (10)$$

where $Q_{Cu(aq)}$ (CBS) (i_{ap} = 0) is the integral of curve b in Fig. 5A and B. A mass balance for the system gives:

$$Q_e(pstat) = n_{aq}Q_{an(aq)} + n_sQ_{an(s)} = Q_e(ICP) \quad (11)$$

Following the lead of previous investigations, it is reasonable to assume that the solid oxide film is Cu_2O (s), formed by an $n = 1$ mechanism, and that the soluble component is Cu(II) (aq). To verify these two hypotheses, a charge balance was performed comparing Q_e(ICP) with Q_e(pstat) for variable applied current (Fig. 6A) and variable time (Fig. 6B). The excellent convergence of both Q_e and Q_m to the line with a slope $n = 1$, demonstrates the validity of the assumptions. Of course, this does not rule out the possibility of Cu (II) in the residual film or Cu(I) in the soluble component as minor components.

Following these results, it is possible to give a kinetic result for Cu dissolution in STW as a function of current at 1200 s (Fig. 7A) and as a function of time at 40 μA (Fig. 7B). Shown is the quantity of soluble Cu, $Q_{Cu(aq)}$ (STW), and the quantity of the residual film, $Q_{Cu(aq)}$ (CBS). The later includes the scale formed by the open circuit reaction. In Fig. 7A we see that Cu_2O is formed preferentially at low current and almost exclusively at open circuit. Cu_2O formation begins to level off around 40 μA and the formation of soluble Cu(II) becomes more significant. The ratio of dissolved Cu(II) to solid Cu_2O approaches 0.8 at 80 μA.

To further verify the formation of the Cu_2O film, XRD and Raman experiments were conducted. Fig. 8 gives the GIXRD pattern for Cu after an anodic pulse of 80 μA for 20 min. It is clear from Fig. 8, that the brown scale [8] on the surface is mainly cuprite. However, we cannot rule out the presence of cupric species either in an amorphous form or present at a depth beyond the penetration of the X-ray photons [8]; the presence of Cu fcc peaks confirm that the X-rays penetrated to the substrate, rather than been isolated by a thick oxide film. *Ex situ* Raman spectroscopy (Fig. 9) was obtained on the same sample, to analyze possible
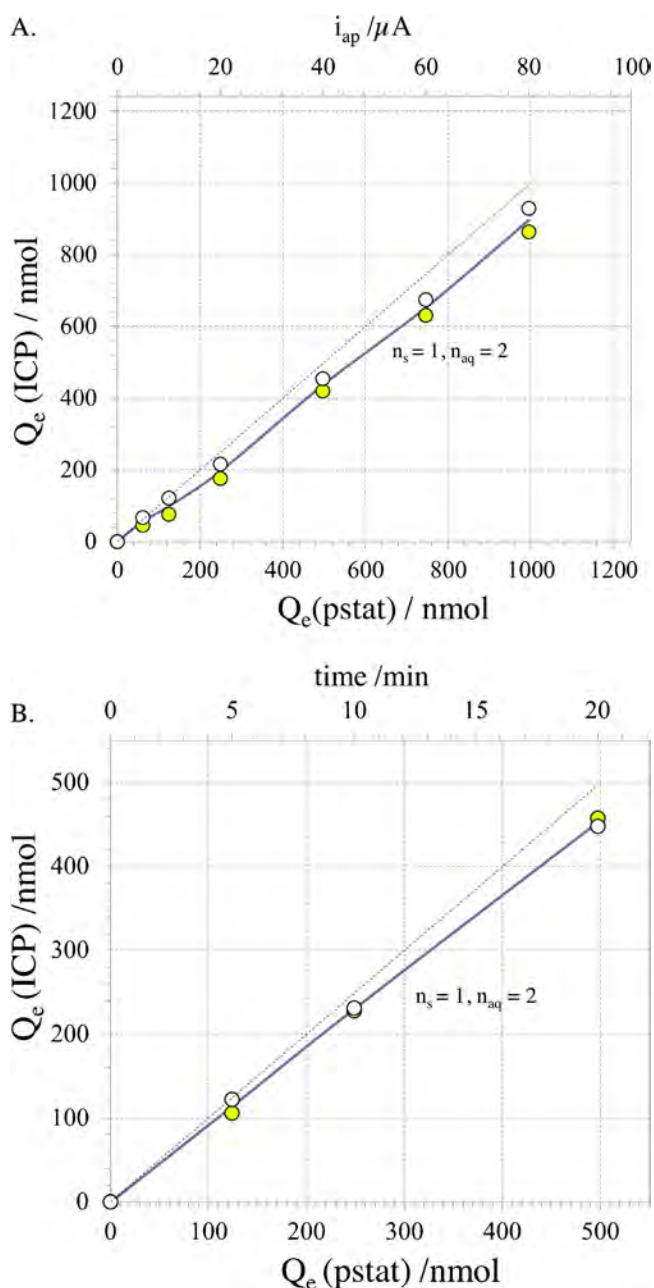

Fig. 6. Q_e(ICP) vs. Q_e(pstat) for (A) variable i_{ap} with Δt = 1200 s; and (B) Variable Δt with i_{ap} = 40 μA. Replicate experiments (marked as colored and hollow ○) were conducted individually. Trend lines were plotted by averaging the replicate experimental data at each current. The dotted line represents a slope = 1 indicating a perfect fit.

crystalline or amorphous species, together with their stoichiometry information. The peaks at 150 cm^{-1}, 220 cm^{-1}, and 650 cm^{-1} proved the existence of Cu_2O, but the main peak of CuO at 650 cm^{-1} is close to that of Cu_2O [52], so identification of CuO is not reliable through this Raman analysis. Yohai et al. [52] proposed that the existence of CuO in Cu_2O would significantly decrease the peak intensity. However, no sign of peak weakness was observed in Fig. 9, which corroborates the AESEC experiment.

3.4. Kinetic analysis

In the previous section we demonstrated that Cu_2O(s) and Cu(II) (aq) are the major products of Cu corrosion either at open circuit or
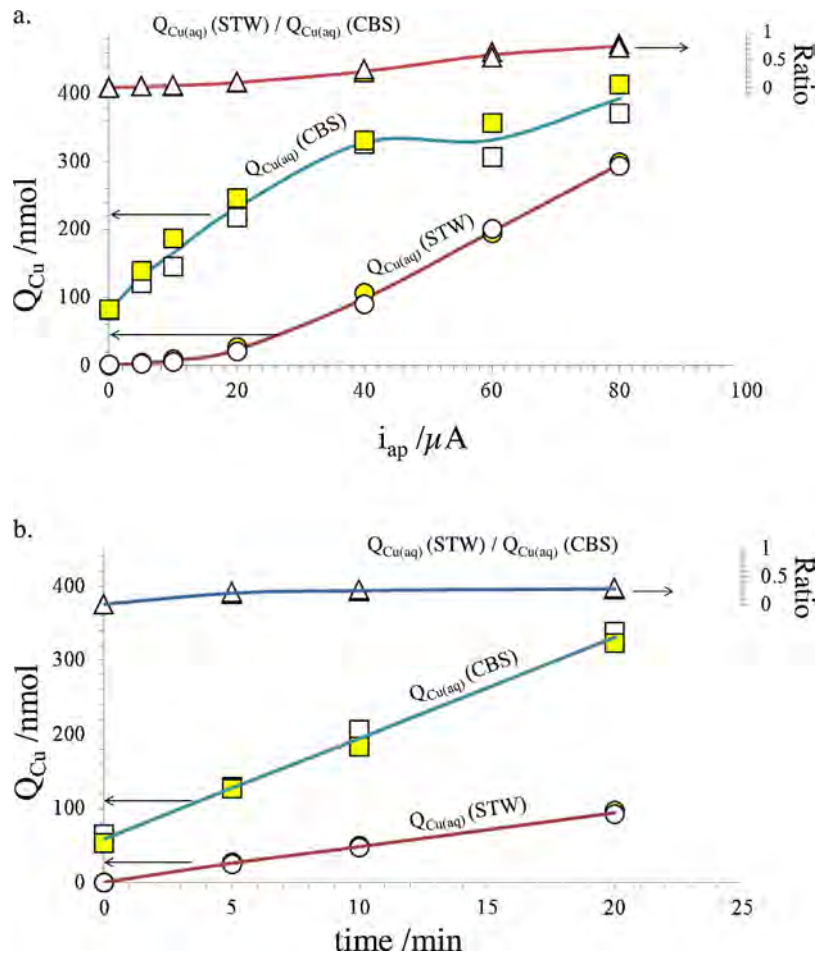
Fig. 7. Comparison between soluble species $Q_{Cu(aq)}(STW)$ ($\bigcirc$), and solid species $Q_{Cu(aq)}(CBS)$ ($\square$). (A) Shown as a function of i_{ap} with $\Delta t = 1200$ s; and (B) as a function of Δt. The ratio of $Q_{Cu(aq)}(STW)/Q_{Cu(aq)}(CBS)$ is shown on a secondary axis. Replicate experiments (marked as colored and hollow $\bigcirc$) were conducted individually. Trend lines were plotted by averaging the replicate experiments.
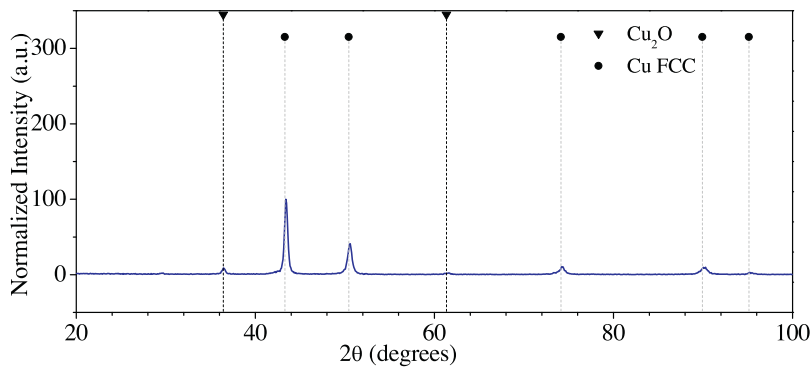

Fig. 8. Grazing incidence X-ray diffraction analysis of copper exposed to STW, being anodically polarized at 80 μA for 20 min.

under anodic polarization in STW. Therefore, from a mass balance, we can write the rates of the elementary reactions for Cu dissolution as:

$$vCu_2O = v_e * -v_{Cu(aq)} \qquad (12)$$

The variation of v_e^*, v_{Cu2O} and $v_{Cu(aq)}$ with time is given in Fig. 10 for 40 μA and 10 μA. The rates of all three reactions rise rapidly to a steady state value. The rates obtained between 900 s and 950 s are shown to the right. In both cases it is observed that all three rates increase simultaneously at $t = 0$ within the time resolution of these

experiments. Only slight changes are observed after 150 s, however it is of interest to note that at 10 μA, $v_{Cu(aq)}$ decreases while v_{Cu2O} increases at longer times. The opposite trend is observed at 40 μA.

Following the review of Section 1, we may describe three different mechanisms for Cu dissolution:
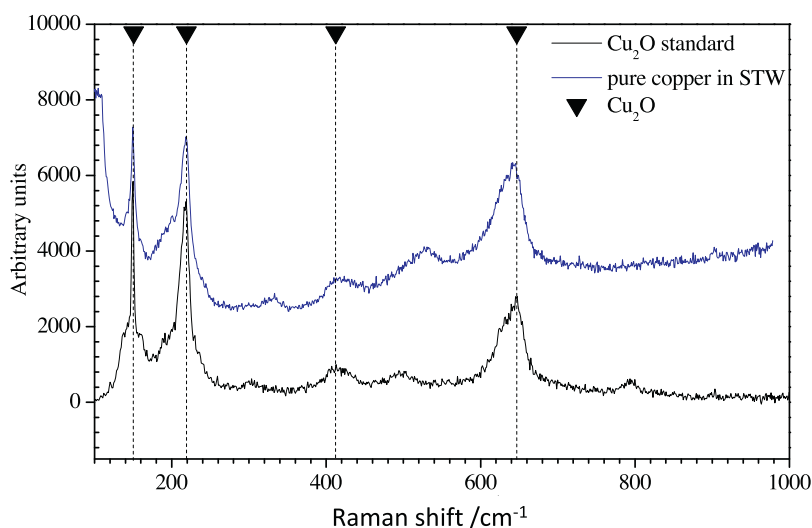
a simultaneous mechanism,

$$2Cu + H_2O \rightarrow Cu_2O + 2e^- + 2H^+ \qquad (13)$$

$$Cu \rightarrow Cu^{2+}(aq) + 2e^-$$
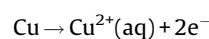
Fig. 9. *Ex-situ* Raman analysis of copper exposed to STW with applied current i_{ap} = 80 μA for 20 min.
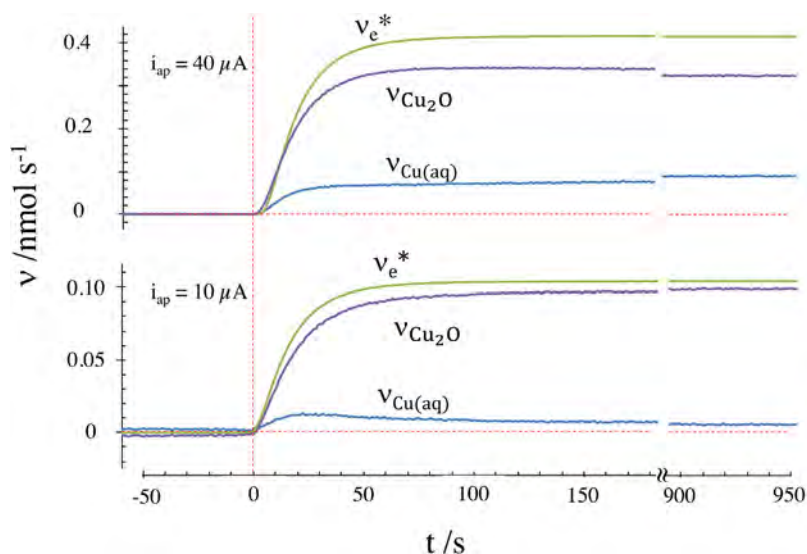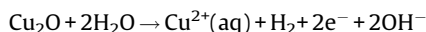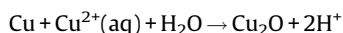

Fig. 10. A kinetic profile for the anodic dissolution of Cu in STW showing electron transfer (v_e), scale formation (v_{Cu2O}), and Cu dissolution ($v_{Cu(aq)}$); at 40 μA and 10 μA.

a sequential mechanism,

$$2Cu + H_2O \rightarrow Cu_2O + 2e^- + 2H^+ \qquad (14)$$

$$Cu_2O + 2H_2O \rightarrow Cu^{2+}(aq) + H_2 + 2e^- + 2OH^-$$

and a redeposition mechanism,

$$Cu \rightarrow Cu^{2+}(aq) + 2e^- \qquad (15)$$

$$Cu + Cu^{2+}(aq) + H_2O \rightarrow Cu_2O + 2H^+$$

Of course these mechanisms represent global reactions that are accessible by AESEC. Intermediate steps involving for example, surface complexation and short lived adsorbed intermediates are not accessible through the measurements presented here and will not be discussed.

It is clear that in both cases of Fig. 10, the dissolution rate rises simultaneously with the electrical current. This would strongly suggest a simultaneous mechanism as proposed in Eq. (13), or at least that the sequential mechanisms are happening on a time scale that is shorter than the time scale of these experiments. Curiously for 10 μA, the dissolution rate rises through a maximum which might be consistent with the dissolution redeposition mechanism of Eq. (15).

4. Conclusion

The results presented here demonstrate that the AESEC method may be used to monitor the kinetics of anodic Cu dissolution. The instantaneous dissolution rate of Cu was measured in real time and compared with the simultaneous measurement of electrochemical current. From a mass/charge balance, it was revealed that the majority species formed during anodic polarization are soluble Cu (II) and insoluble Cu(I). The insoluble species was quantified after the experiment by dissolution in a citrate buffer solution.

The solid corrosion products were characterized by Raman and XRD analysis which confirmed that a Cu_2O film forms on the Cu surface at open circuit and during anodic polarization. Quantitative relationships of Cu(I), Cu(II) species vs. applied current and vs. time

duration of galvanostatic pulse were presented. Knowledge of the n values for the elementary reactions permit a real time mass balance between the electrical anodic current and the Cu dissolution rate so that the rates of formation of Cu2O (s) and Cu(II) (aq) may be estimated in real time. The results presented here are consistent with the solid and aqueous species being formed simultaneously (on the time scale of this experiment) rather than by a sequential or a redeposition mechanism.

Acknowledgements

References

[1] Word Health Organization, Copper in drinking-water, Background document for development of WHO Guidelines for Drinking-water Quality, WHO/SDE/WSH/03.04/88.

[2] V.F. Lucey, Mechanism of pitting corrosion of copper in supply waters, British Corrosion Journal 2 (1967) 175–185.

[3] M.A. Edwards, T.E. Meyer, et al., Role of inorganic anions, NOM, and water treatment processes in copper corrosion, AWWARF, Denver, USA, 1996.

[4] T.H. Merkel, H.J. Groß, W. Werner, T. Dahlke, S. Reicherter, G. Beuchle, S.H. Eberle, Copper corrosion by-product release in long-term stagnation experiments, Water Research 36 (2002) 1547–1555.

[5] R.A. Isaac, L. Gil, A.N. Cooperman, K. Hulme, B. Eddy, M. Ruiz, K. Jacobson, C. Larson, O.C. Pancorbo, Corrosion in drinking water distribution systems: a major contributor of copper and lead to wastewaters and effluents, Environmental science & technology 31 (1997) 3198–3203.

[6] N. Boulay, M. Edwards, Role of temperature, chlorine, and organic matter in copper corrosion by-product release in soft water, Water Research 35 (2001) 683–690.

[7] M. Fabbricino, Copper release in drinking water due to internal corrosion of distribution pipes, Global NEST Journal 7 (2005) 163–171.

[8] W. Xiao, S. Hong, Z. Tang, S. Seal, J.S. Taylor, Effects of blending on surface characteristics of copper corrosion products in drinking water distribution systems, Corrosion Science 49 (2007) 449–468.

[9] A.E. Broo, B. Berghult, T. Hedberg, Copper corrosion in water distribution systems–the influence of natural organic matter (nom) on the solubility of copper corrosion products, Corrosion Science 40 (1998) 1479–1489.

[10] D.A. Lytle, M.N. Nadagouda, A comprehensive investigation of copper pitting corrosion in a drinking water distribution system, Corrosion Science 52 (2010) 1927–1938.

[11] M. Edwards, J.F. Ferguson, S.H. Reiber, The pitting corrosion of copper, Journal of the American Water Works Association 86 (1994) 74–90.

[12] M. Edwards, T. Meyer, J. Rehring, Effect of selected anions on copper corrosion rates, Journal of the American Water Works Association 86 (1994) 73–81.

[13] A.E. Broo, B. Berghult, T. Hedberg, Copper corrosion in drinking water distribution systems – the influence of water quality, Corrosion Science 39 (1997) 1119–1132.

[14] H.P.K. Andrew, Y.Y. Macauley, Corrosion and leaching of copper tubing exposed to chlorinated drinking water, Water, Air, and Soil Pollution 108 (1998) 457–471.

[15] G. Hultquist, L. Gråsjö, Q. Lu, T. Åkermark, The analysis of gas consumption in the reaction of Fe and Cu in $H_2^{16}O/H_2^{18}O/O_2$ gas mixtures, Corrosion Science 36 (1994) 1459–1471.

[16] T.M.H. Saber, A.A.E. Warraky, Electrochemical and spectroscopic studies on dezincification of α brass: Part 1: Effect of pretreatment on surface composition of 70-30 α brass, Corrosion Engineering, Science and Technology 26 (1991) 279–285.

[17] Y. Feng, K.S. Siow, W.K. Teo, K.L. Tan, A.K. Hsieh, Corrosion mechanisms and products of copper in aqueous solutions at various pH values, Corrosion 53 (1997) 389–398.

[18] J.M. Bastidas, A. López-Delgado, E. Cano, J.L. Polo, F.A. López, Copper corrosion mechanism in the presence of formic acid vapor for short exposure times, Journal of the Electrochemical Society 147 (2000) 999–1005.

[19] A. Palit, S.O. Pehkonen, Copper corrosion in distribution systems: evaluation of a homogeneous Cu_2O film and a natural corrosion scale as corrosion inhibitors, Corrosion Science 42 (2000) 1801–1822.

[20] Y.H. Lu, H.B. Xu, J. Wang, et al., Oxygen reduction mechanism on copper in a 0.5 M H_2SO_4, Electrochimica Acta 54 (2009) 3972–3978.

[21] T. Hurlen, Dissolution of cuprous chloride in acid chloride solution, Acta Chemica Scandinavica 16 (1962) 279–282.

[22] T. Hurlen, Film growth on copper in acidified cupric chloride solutions, Acta Chemica Scandinavica 15 (1961) 1246–4254.

[23] H. Lal, H.R. Thirsk, The anodic behaviour of copper in neutral and alkaline chloride solutions, Journal of the Chemical Society (Resumed) 538 (1953) 2638–2644.

[24] T. Aastrup, M. Wadsak, M. Schreiner, C. Leygraf, Experimental in situ studies of copper exposed to humidified air, Corrosion Science 42 (2000) 957–967.

[25] P.K. Hong, Y.Y. Macauley, Corrosion and leaching of copper tubing exposed to chlorinated drinking water, Water, Air, and Soil Pollution 108 (1998) 457–471.

[26] H. Cong, H.T. Michels, J.R. Scully, Passivity and pit stability behavior of copper as a function of selected water chemistry variables, Journal of the Electrochemical Society 156 (2009) C16–C27.

[27] E. Mattsson, Counteraction of pitting in copper water pipes by bicarbonate dosing, Materials and Corrosion 39 (1988) 499–503.

[28] M. Drogowska, L. Brossard, H. Ménard, Influence of anions on the passivity behavior of copper in alkaline solutions, Surface and Coatings Technology 34 (1988) 383–400.

[29] G. Schmitt, P. Plagemann, E. Slavcheva, ECN-measurements at copper in artificial tap water–Investigation of anion-effects, Materials and Corrosion 52 (2001) 439–444.

[30] Y.P. Feng, S.K. Sinha, C.A. Melendres, D.D. Lee, X-ray off-specular reflectivity studies of electrochemical pitting of Cu surfaces in sodium bicarbonate solution, Physica B: Condensed Matter 221 (1996) 251–256.

[31] S.A. Imran, J.D. Dietz, G. Mutoti, J.S. Taylor, A.A. Randall, Modified Larsons ratio incorporating temperature, water age, and electroneutrality effects on red water release, Journal of Environmental Engineering 131 (2005) 1514–1520.

[32] E.J. Singley, The search for a corrosion index, Journal of American Water Works Association 73 (1981) 579–582.

[33] J.R. Rossum, T.M. Douglas, An evaluation of the calcium carbonate saturation indexes, Journal of American Water Works Association 75 (1983) 95–100.

[34] E. Sarver, K. Dodson, R.P. Scardina, R. Lattyak-Slabaugh, M. Edwards, C. Nguyen, Copper pitting in chlorinated, high-pH potable water, Journal of American Water Works Association 103 (2011) 86–98.

[35] H. Cong, J.R. Scully, Effects of aluminum solids on the under deposit corrosion of copper in synthetic potable water: the arguments for and against a semi-permeable membrane, Journal of the Electrochemical Society 160 (2013) C403–C413.

[36] Y. Feng, W.K. Teo, K.S. Siow, K.L. Tag, A.K. Hsieh, The Corrosion Behavior of Copper in Neutral Tap Water. Part I: Corrosion Mechanisms, Corrosion Science 38 (1996) 369–385.

[37] M. Drogowska, L. Brossard, H. Ménard, Copper Dissolution in $NaHCO_3$ and $NaHCO_3$ + NaCl Aqueous Solutions at pH 8, Journal of Electrochemical Society 139 (1992) 39–47.

[38] S. Nakayama, Mechanistic study by electrochemical impedance spectroscopy on reduction of copper oxides in neutral solutions, SEI Technical Review (2009) 62–68.

[39] G. Hultquist, Hydrogen evolution in corrosion of copper in pure water, Corrosion Science 26 (1986) 173–177.

[40] P. Szakalos, G. Hultquist, G. Wikmark, Corrosion of copper by water, Electrochemical and Solid-State Letters 10 (2007) C63–C67.

[41] G. Hultquist, P. Szakálos, M.J. Graham, G.I. Sproule, G. Wikmark, Detection of hydrogen in corrosion of copper in pure water, In International Corrosion Congress (2008) paper No. 3884.

[42] G. Hultquist, P. Szakálos, M.J. Graham, A.B. Belonoshko, G.I. Sproule, L. Gråsjö, P. Dorogokupets, B. Danilov, T.A. Astrup, G. Wikmark, G.-K. Chuah, J.-C. Eriksson, A. Rosengren, Water corrodes copper, Catalysis Letters 132 (2009) 311–316.

[43] J.P. Simpson, R. Schenk, Hydrogen evolution from corrosion of pure copper, Corrosion Science 27 (1987) 1365–1370.

[44] T.E. Eriksen, P. Ndalamba, I. Grenthe, On the corrosion of copper in pure water, Corrosion Science 29 (1989) 1241–1250.

[45] L.O. Werme, P.A. Korzhavyi, Comment on Hultquist et al. 'Water Corrodes Copper' [Catal. Lett. 132 (2009) 311], Catalysis Letters 135 (2010) 165–166.

[46] S. Jacobs, M. Edwards, Sulfide scale catalysis of copper corrosion, Water Research 34 (2000) 2798–2808.

[47] C. Ackfeld, O. von Franqué, W. Siedlarek, Electrochemical potential measurements of commercial copper tubes with different surfaces, Materials and Corrosion 48 (1997) 624–630.

[48] K. Ogle, Atomic emission spectroelectrochemistry: a new look at the corrosion, dissolution and passivation of complex materials, EuroCorr 2011, Stockholm, Sweden, 2011, pp. 60–67.

[49] K. Ogle, S. Weber, Anodic dissolution of 304 stainless steel using atomic emission spectro-electrochemistry, Journal of the Electrochemical Society 147 (2000) 1770–1780.

[50] V. Shkirskiy, P. Marciel, J. Deconinck, K. Ogle, On the time resolution of the atomic emission spectroelectrochemistry method, Journal of electrochemical society 163 (2016) C1–C8.

[51] J. Lin, M.Z. Liu, (1995) Detergent for steel aluminium and copper materials, CN1101950 (A) (in Chinese).

[52] L. Yohai, W.H. Schreiner, M. Vázquez, M.B. Valcarce, Surface characterization of copper: zinc and brass in contact with tap water inhibited with phosphate ions, Applied Surface Science 257 (2011) 10089–10095.